Journal of Molecular Catalysis A: Chemical 310 (2009) 101–112

Contents lists available at ScienceDirect

Journal of Molecular Catalysis A: Chemical

journal homepage: www.elsevier.com/locate/molcata

The influence of the active component and support nature, gas mixture composition on physicochemical and catalytic properties of catalysts for soot oxidation

Aleksandra S. Ivanova*, Galina S. Litvak, Vladimir V. Mokrinskii, Lyudmila M. Plyasova, Vladimir I. Zaikovskii, Vasilii V. Kaichev, Aleksandr S. Noskov

Boreskov Institute of Catalysis SB RAS, Pr. Akad. Lavrentyeva 5, Novosibirsk 630090, Russia

ARTICLE INFO

Article history:
Received 7 April 2009
Received in revised form 3 June 2009
Accepted 3 June 2009
Available online 10 June 2009

Keywords:
Soot
Oxidation
Catalyst
Active component (M–Mn–O, M = Ce, Fe)
Support (gamma-, theta-, alpha-Al_2O_3, SiO_2)
Thermal evolution
Gas mixture composition

ABSTRACT

Physicochemical and catalytic properties of compositions Fe(Ce)–Mn–O/support (gamma-, theta-, alpha-Al_2O_3, SiO_2 as the support) and Pt/CeO_2/theta-Al_2O_3 for oxidation of soot were characterized. It was established that the phase composition of the initial catalysts depended mainly on the nature of the active component and preparation conditions. Non-isothermal treatment of the soot–catalyst compositions at the temperature up to 1000 °C resulted in a change in the phase composition depending mainly on the final treatment temperature. The catalyst surface area was determined by the support nature. It was established that catalyst activities for oxidation of soot are determined by both catalyst nature and composition of gas mixture. The process of the soot oxidation is thought to involve oxygen from the catalyst surface. The higher proportion of weakly bound surface oxygen, the higher was the catalyst activity. An increase in the oxygen concentration from 5% O_2/N_2 to 15% O_2/N_2 is shown to lead to a decrease of the temperature of the soot oxidation. The influence of the oxygen concentration on the process of soot oxidation becomes weaker in the presence of water vapor. Results showed that the presence of NO in the gas mixture favors a decrease in the oxidation temperature of the soot, the higher being the nitrogen oxide concentration, the more pronounced effect. Introduction of SO_2 in amount of 50 ppm in the gas mixture has no noticeable effect on the process of the soot oxidation. Among the catalysts under study, Fe–Mn–K–O/gamma-Al_2O_3 is most effective to oxidation of the soot at otherwise identical conditions.

1. Introduction

Automotive exhausts, in particular those of diesel engines, contain hydrocarbons (HC), carbon oxides, nitrogen oxides and soot aerosols. It is commonly accepted that catalytic methods are most effective for neutralization of these pollutions. Currently, catalytic devices allow one to remove HC, CO, NO_x from exhaust gas in stoichiometrically controlled, spark-ignition engines. However, a more severe problem is the removal of soot aerosol (soot) from diesel engines. At present cleaning from soot is mainly achieved by capturing it by ceramic filters. The difficulty is that the soot particles are very small in size ($d < 0.5$ μm) and have low density in the exhaust flow [1].

The problem of soot neutralization can be resolved, for example, using a catalytic bed filter. It was suggested [2–5] to use systems based on eutectic salt mixtures with low melting temperatures, among which are oxides or sulfates of molybdenum, vanadium, cesium (Cs_2MoO_4–V_2O_5; $CsVO_3$–MoO_3; Cs_2SO_4–V_2O_5, etc.), to provide a good contact between the catalyst and soot. In this case the soot starts oxidizing at ca. 350 °C and the maximal oxidation rate is reached at 537–577 °C [6]. The main drawback of the systems is that individual catalyst components may evaporate at certain temperatures to make the catalyst composition and, consequently, the activity to soot oxidation altered. In addition, these systems are soluble in liquid water, so the active component could be lost by leaching [7]. Supported catalytic systems for the soot oxidation, such as CuO/CeO_2 [8], Cu–V–K/α-Al_2O_3, $Cs_4V_2O_7/SiO_2$–Al_2O_3 [9,10], MoO_3/SiO_2, V_2O_5/SiO_2 [11], are also attractive to researchers. However, one can hardly compare their efficiencies because different methods are used for estimation of their activities. The search for active and stable catalytic compositions for the soot oxidation is in progress.

The soot in exhaust gases of diesel engines comprises adsorbed hydrocarbon molecules and a liquid phase (condensed hydrocarbons and sulfuric acid) [12]. The sulfuric acid is formed in the exhaust gases upon combustion of sulfur-containing components of diesel fuels, sulfur being oxidized to SO_2 and a part of SO_2 (ca. 2%) is oxidized to SO_3. Water vapor involved in the exhaust gases reacts

* Corresponding author. Tel.: +7 383 326 97 72; fax: +7 383 330 80 56.
E-mail address: iva@catalysis.ru (A.S. Ivanova).

1381-1169/$ – see front matter © 2009 Elsevier B.V. All rights reserved.
doi:10.1016/j.molcata.2009.06.004

rapidly with SO_3 to produce sulfuric acid. Some authors report the soot composition as 89–99 wt% of carbon, 0.3–0.5 wt% of hydrogen, 0.1–1.0 wt% of oxygen, 0.1–1.1 wt% of sulfur, up to 0.5 wt% of mineral compounds [13], while other authors report this composition as 66.1 wt% of carbon, 3.6 wt% of hydrogen, 2.4 wt% of nitrogen, 24.1 wt% of oxygen, 2 wt% of sulfur [8]. Diesel soot compositions appear to be highly variable. Again, it is mentioned in Ref. [8] that the real soot comprises not only the solid carbon fraction but also volatile fractions due to inclusion of hydrocarbons (the nature of which depends on the type of fuel used and the amount of additives) in the solid phase. Non-isothermal treatment of the soot gives rise to both low- and high-temperature exoeffects in the DTA curves that indicate oxidation of the soot 'fractions'. As to oxidation of model soot Printex U, only high-temperature exoeffect is observed at 620 °C [14]. Therefore, the efficiency of catalysts for the soot oxidation can only be estimated when the chosen model is most similar to the real diesel soot.

It is well known [15] that the air/fuel ratio changes at different modes of diesel engine operation and the fuel combustion is accompanied by formation of water vapor. These factors affect not only the composition of the exhaust gases but also the activity and stability of the catalyst or catalytic neutralizer. Emissions from diesel engines contain soot and nitrogen oxides as main pollutants. NO_2 is one of the best oxidants of soot particles; NO_2 is initiated by the formation of active oxygen in the gas phase in the presence of NO and O_2. A synergistic effect is observed as a result of surface nitrate decomposition, which results in gas phase NO_2 and desorption of active oxygen. Active oxygen is likely to play a role on the acceleration of the soot oxidation and to contribute more than desorbed NO_2 or NO_2 from the surface nitrate decomposition [16]. The specific features of fuel burning in diesel engines make it necessary to study the influence of the gas mixture composition on the oxidation of soot in the presence of a catalyst.The present paper describes the studies of physicochemical and catalytic properties for the soot oxidation of systems comprising active components and supports of different natures and in different amounts; the influence of concentrations of oxygen, nitrogen oxide, sulfur dioxide and water vapor on the oxidation of soot.

2. Experimental

2.1. Catalyst preparation

Two methods were used for preparation of catalyst catalysts. The first one (I) is based on a deposition of nitrates of elements taken in a certain ratio with ammonia solution at certain pH 8.8 ± 0.2 and temperature of (70 ± 2) °C on γ-Al_2O_3. The alumina support material was ground previously in a planetary grinding-mill into particles of 5–10 μm in size. A suspension obtained was kept at given conditions for 30 min and then filtered. Resulting suspensions were filtered out, and precipitates were washed with distilled water. The second method (II) is based on an incipient wetness impregnation of supports with a nitrate solution. All the samples were dried at 110–120 °C for 12–14 h in air and subjected to thermal treatment in dry air flow at 400 or 500 °C for 4 h. γ-, θ- and α-alumina and silica were used as supports. Basic characteristics of the supports are given in Table 1.

The deposition of soot on catalyst or support is based on mixing of 20% soot and 80% catalyst (support), fraction 0.25–0.5 mm, through suspending in acetone that was subsequently to be then evaporated.

2.2. Catalyst characterization

The content of the main components was determined by the atomic absorption spectrometry [17] with an accuracy of 0.01–0.03%.

X-ray powder diffraction (XRD) patterns of the catalysts were obtained with an URD-63 diffractometer using Cu K_α radiation. A reflected beam graphite monochromator was used for filtration of the Cu K_β radiation. The analysis was carried out in a stepwise mode with the step of $2\theta = 0.05–0.1°$ and storage time of 20–30 s depending on the degree of a sample crystallinity. To identify the phase composition, the data obtained for d_i (interplane distances) and I_i (relative intensity of diffraction maxima) were compared to the reference data [18].

Chemical composition of the catalyst surface was determined by X-ray photoelectron spectroscopy (XPS). The experiments were performed on a VG ESCALAB HP electron spectrometer using non-monochromatic Al K_α radiation ($h\nu = 1486.6$ eV). Gold and copper standards ($Au4f_{7/2}$ at 84.0 eV and $Cu2p_{3/2}$ at 932.6 eV) were used to verify spectrometer calibration. Catalyst samples were mounted on a sample holder using a two-sided adhesive tape. Charging of the samples was accounted for by setting the peak of the Si2p signal to 103.4 eV.

The specific surface area (*SSA*) was determined with an accuracy of ±10% by the heat desorption of argon [19].

Particle size distribution in the soot was studied using a JEM-2010 electron microscope with a resolution of 0.14 nm. Before measurements samples were prepared by ultrasonicating a small quantity of the powder for a few minutes in ethanol. The resultant slurry was then deposited on a copper grid.

Thermal evolution of the individual soot and soot deposited on supports or catalysts was studied in a controlled atmosphere using a derivatograph Q1500D. Samples weighing 100 mg (20% soot + 80% catalyst, fraction 0.25–0.5 mm) were studied in the ranges from room temperature (18–21 °C) to 1000 °C. An experimental accuracy was ±5 °C for temperature and 0.25 mg for weight loss at the balance sensitivity of 50 mg.

A home-made setup was used for kinetic studies of the soot oxidation in the presence of α-Al_2O_3 or a catalyst. The catalytic activity for the oxidation of soot was quantified during temperature programmed oxidation (TPO) of catalyst–soot mixtures. The catalyst-containing sample was heated from 50 to 700 °C using a programmed linear temperature elevation from 50 to 700 °C at a rate of 5 °C/min. The sample was kept at 700 °C for 10 min. Outlet gas aliquots were obtained every 3 min for GC analysis using a Kristall-2000M chromatograph equipped with a flame ionization detector with methanator was used for CO and CO_2 and a thermoconductivity detector for O_2 and H_2O. A catalyst sample weighing 100 mg (20% soot −80% catalyst, fractions 0.25–0.50 mm) was loaded into a quartz reactor mounted in a furnace in the setup and connected to inlet and outlet lines of the gas or gas–vapor reactant mixture.

Table 1
Characteristics of supports.

Support	Calcination temperature (°C)	Phase composition[a]	*SSA* (m^2/g)	Bulk density (g/cm^3)
γ-Al_2O_3	650	γ-Al_2O_3: $a = 0.793$ nm;	200	0.62
θ-Al_2O_3	1000	θ-Al_2O_3: $a = 1.186$, $b = 0.291$, $c = 0.562$ nm	106	–
α-Al_2O_3	1250	α-Al_2O_3: $a = 0.478$; $c = 1.304$ nm	8	1.09
SiO_2	1250	X-ray amorphous	0.5	0.19

[a] a and c are unit cell constants.

Table 2
Characteristics of catalysts.

#	Catalyst		Method	T_{calc} (°C)	Active comp. (wt%)	M/Mn(Co) ratio (wt)		*SSA* (m^2/g)
	Support	Active component				Calc.	Exp.	
1	α-Al_2O_3	Ce–Mn–O	II	400	10.1	2	1.69	24
2	γ-Al_2O_3	Ce–Mn–O	II	400	19.5	2	1.45	145
3	γ-Al_2O_3	Fe–Mn–O	I	400	47.9	1	1.23	290
4	γ-Al_2O_3	Fe–Mn–K–O	I	400	55.5 (K_2O = 7.6)	1	1.23	200
5	γ-Al_2O_3	Fe–Mn–Cs–O	I	400	54.5 (Cs_2O = 13.4)	1	1.23	220
6	SiO_2	Fe–Mn–K–O	II	400	19.9 (K_2O = 2.6)	1	1.23	28
7	SiO_2	Fe–Mn–Cs–O	II	400	21.7 (Cs_2O = 3.1)	1	1.25	40
8	θ-Al_2O_3	Ce–O	II	500	11.7	–	–	95
9	θ-Al_2O_3	Pt–Ce–O	II	500	10.1 (Pt = 1.5)	–	–	92

The soot was oxidized in the reactor with various gas mixtures fed therein.

3. Results and discussion

3.1. Chemical composition and thermal behavior of the soot

The samples prepared for studying the process of catalyzed soot oxidation differ by the nature and concentration of the active component, as well as by the support nature, preparation conditions and treatment temperature.

Standard parameters were characteristic of the supports (γ-, θ- and α-Al_2O_3) (Table 1): γ-Al_2O_3 structured as defect cubic spinel, a = 0.793 nm, the coherent scattering regions (CSR) ~5–7 nm; θ-Al_2O_3 structured as monoclinic, a = 1.186, b = 0.291, c = 0.562 nm, CSR ~20–22 nm; α-Al_2O_3 structured as hexagonal, a = 0.476 nm, c = 1.3 nm, CSR ~100 nm. SiO_2 is X-ray amorphous. As seen from Table 1, the specific surface area of the supports lies in the range 0.5–200 m^2/g.

Table 2 shows basic characteristics of the catalysts. A good agreement between the calculated and experimental constituent ratio in the active component is observed for most of the catalysts. For catalysts prepared by impregnation (*method II*), *SSA* of the catalyst is controlled mainly by the *SSA* of the support. For catalysts prepared by method I, *SSA* lies in the range 200–290 m^2/g. *SSA* is determined by the nature of the components. A larger *SSA* (290 m^2/g) is characteristic of the catalysts Fe–Mn–O/γ-Al_2O_3 prepared by method I. However, the introduction of potassium or cesium in this sample leads to the decrease of the *SSA* up to 200–220 m^2/g.

The soot sample consisting of globular particles of 20–50 nm in size (Fig. 1) was chosen for studying the catalyst efficiency in the process of soot oxidation. The soot particles are linked to one another to form extended chains and aggregates. According to XRD data (Fig. 2), the soot particles are structured as turbostratic graphite, i.e. graphite with hexagonal carbon networks stacked in random manner along [0 0 1] direction, layer disordering being γ = 100%. CSR are 1.2–1.5 nm in average size along [0 0 2] direction and ca. 2 nm along [h k 0] directions. That means stacking of three or four graphite networks with cross-dimension of ca. 2 nm within one CSR. The transmission electron microscope (TEM) studies of catalyst–soot compositions (with Ce–Mn–O/α-Al_2O_3 and Ce–Mn–O/γ-Al_2O_3 samples chosen as catalysts, see Table 2) reveal that the soot particles are shaped as globules of 20–50 nm in size (Fig. 3), i.e. they are practically identical in size with individual soot particles. Both the individual soot and the soot supported on the catalyst are completely identical in morphology. The high-resolution micrograph (Fig. 4) shows that the soot structure is made up by short fragments of spherically symmetrical graphite layers (l = 1–2 nm) to form a globular particle.

Electron micrographs of the soot–Ce–Mn–O/α-Al_2O_3 composition (Fig. 3a) reveal soot particles along with the catalyst particles, which are crystalline α-Al_2O_3 particles (≥100 nm in size) with dispersed active component particles (Ce–Mn–O) distributed through the oxide surface, the active component particles being poly-

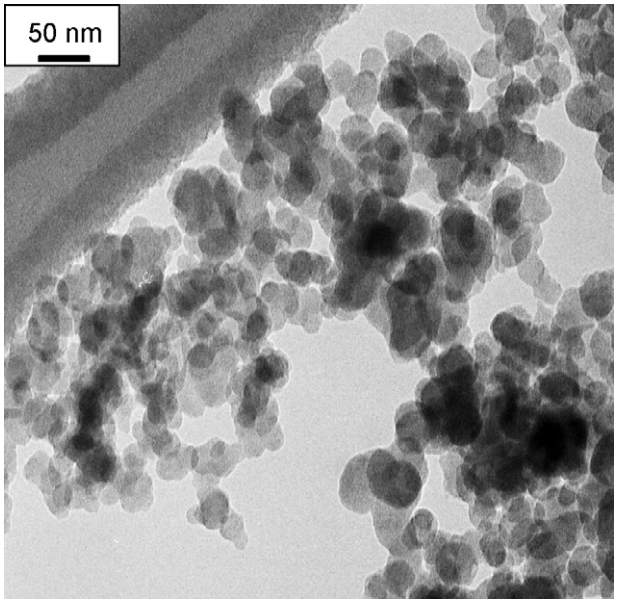

Fig. 1. TEM image of the original soot.

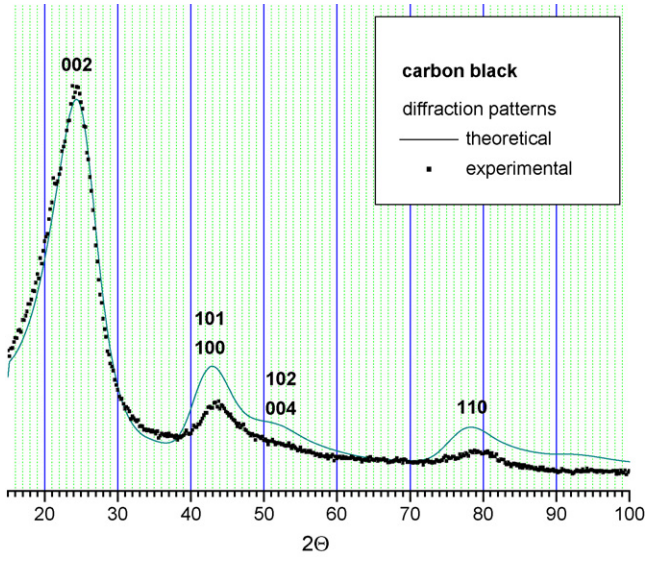

Fig. 2. XRD pattern of soot sample: the comparison of experimental (····) and calculated XRD patterns; theoretically for turbostrate graphite with given distribution parameters.

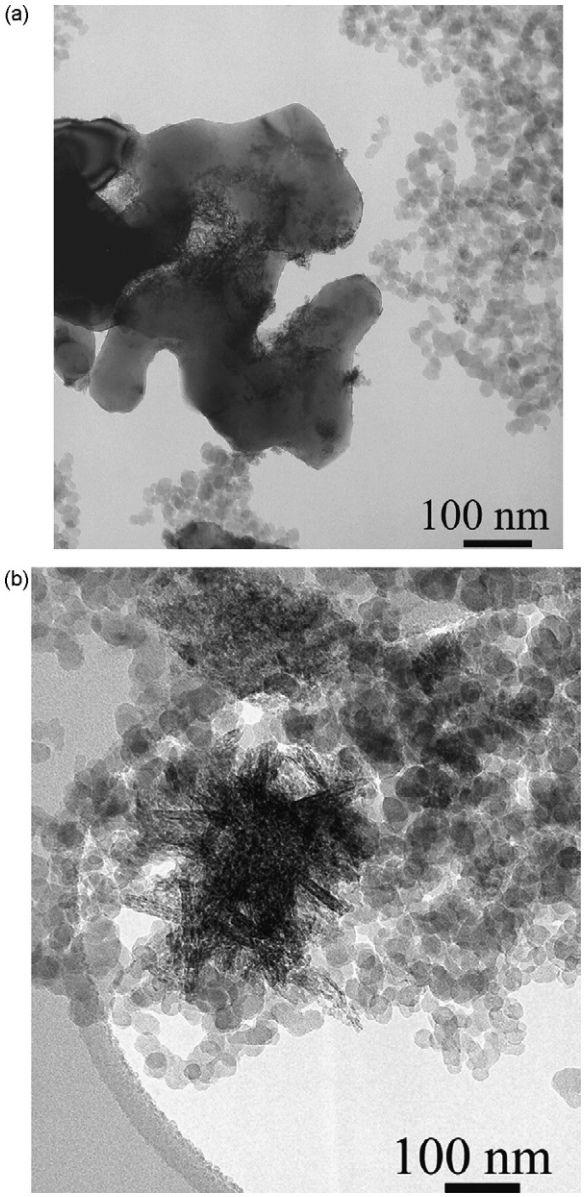

Fig. 3. TEM image of soot–Ce–Mn–O/α-Al_2O_3 (a) and soot–Ce–Mn–O/γ-Al_2O_3 (b).

crystalline aggregates of primary bricks of ca. 5 nm in size. The Ce–Mn–O/γ-Al_2O_3 sample (Fig. 3b) is seen as porous crystalline aggregates (no less than 100 nm in size) built-up by primary needle bricks (d = 5–10 nm and l = 20–50 nm). Hence, it is shown that

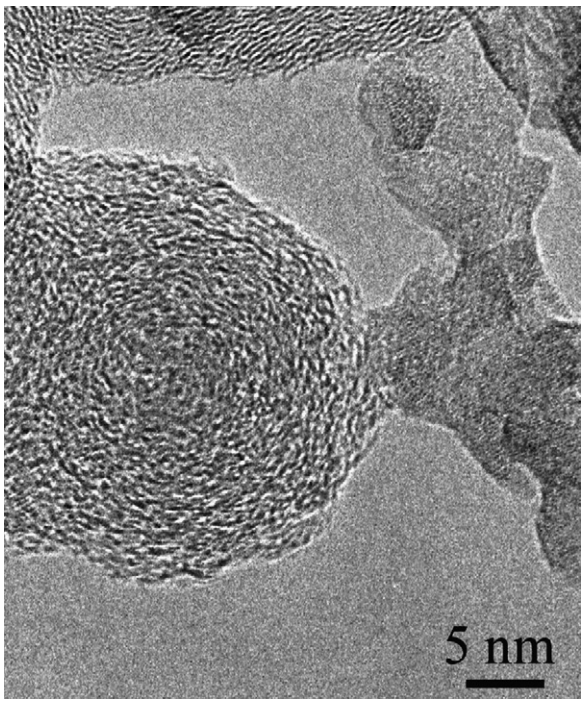

Fig. 4. High resolution TEM image of soot–Ce–Mn–O/α-Al_2O_3 composition.

the suggested procedure for the soot deposition on the catalyst surface does not affect particle size and morphology both of the soot and of the catalyst.

Thermal behavior of the individual soot and the soot in the presence of supports or catalysts is studied in the reaction mixture fed at 5 L air/h. The oxidation of supported soot is seen (Fig. 5) to start at a lower temperature than oxidation of soot by itself. However, the temperature difference is no more than 25–30 °C, while the amount of removed soot is ca. 20% higher in the presence of γ-Al_2O_3. It is reasonable to suppose that such an "increase" is related to contribution of water removed due to dehydroxylation of γ-Al_2O_3 at elevated temperature.

The soot oxidation is more effective in the presence of catalysts (Table 3). With impregnated Ce–Mn–O/α-Al_2O_3 systems as the catalysts, the soot ignition temperature ($T_{ign.}$) being 345 °C; it is ca. 100 °C lower than that of soot alone (Table 3), the exoeffect temperature is 580 °C. At the same time, doubling the active component loading or supporting it on γ-Al_2O_3 has a detrimental effect on the soot oxidation parameters. Notice that application of γ-Al_2O_3-based catalysts results not only in a more considerable decrease in the ignition temperature but also it results in changes in the shape and position of chief exoeffect in DTA curves (Table 3). Again, a

Table 3
Influence of the nature and content of the active component on the soot burning in the gas mixture containing 5 L air/h.

#	Support	Active component		Temp. of soot ignition (DTG) (°C)	Temp. of exoeffect T_{DTA} (°C)	Weight losses, TG		
		Chemical composition	Content (%)			H_2O (%)	Soot	
							mg	%
1	–	–	–	435	620	0	18.5	92.5
2	α-Al_2O_3	Ce–Mn–O	10.1	345	580	0.5	15.5	77.5
3	γ-Al_2O_3	Ce–Mn–O	19.5	360	620	3.5	20.5	103
4	γ-Al_2O_3	Fe–Mn–O	47.9	380	610	6.5	16.5	82.5
5	γ-Al_2O_3	Fe–Mn–K–O	55.5	190, 340	410, 540	3.0	20.0	100
6	γ-Al_2O_3	Fe–Mn–Cs–O	54.5	180, 330	440, 580	6.0	22.0	110
7	SiO_2	Fe–Mn–K–O	19.9	190, 355	440/520	1.0	22.5	110
8	SiO_2	Fe–Mn–Cs–O	21.7	185, 365	425, 520, 570	0.75	19.3	96.5
9	θ-Al_2O_3	Ce–O	11.7	360	415/625	2.0	16.5	82.3
10	θ-Al_2O_3	Pt–Ce–O	10.1 (Pt = 1.5)	395	585/610	1.1	19.2	96.0

"higher" amount of soot removed (103%) is also observed in the case of these catalysts that may be related to the contribution of water removed concurrently from the support, as mentioned above.

Deposition of Fe–Mn–O in amount of ca. 50 wt% on γ-Al_2O_3 does not also allow the oxidation process to be accelerated (Table 3). However, the promotion of this sample with potassium or cesium through impregnation of Fe–Mn–O/γ-Al_2O_3 dried at 110 °C with aqueous potassium or cesium nitrate solution provides lowering of the ignition temperature to 180–190 and 330–340 °C, respectively (Table 3). Two exoeffects at 410–440 °C and 540–580 °C are observed instead of single exoeffect at 620 °C.

The fact that potassium or cesium promoters affect so remarkably the process of soot burning may be accounted for changes in the Fe–O or Mn–O bond strength in the presence of these cations [20] that results in an increase in the oxygen mobility and efficiency of the soot oxidation. Other researchers have found that alkali elements can promote the soot oxidation [21–23]. Substitution of SiO_2 for γ-Al_2O_3 (Table 3) in the catalysts under consideration has no detrimental effect on the catalytic performance in the soot oxidation at even lower loading of the active component.

Special interest presented inflicted Ce-containing samples (CeO_2/θ-Al_2O_3, Pt/CeO_2/θ-Al_2O_3). First, it is well known that oxygen is the most obvious, since it is present in large quantities (5–10%) in diesel exhausts. Therefore, oxygen storage/release materials such as CeO_2 [24–26] can provide active oxygen. Second, the interphase interaction takes place between platinum and CeO_2 that, perhaps, leads to stabilization of an ionic state of platinum [27]. Thirdly, according to data reported in Refs. [28,29], platinum can take part in redox processes, namely:

$$NO + (1/2)O_2 \xrightarrow{Pt} NO_2$$

$$CeO_2 + \text{“C”} \rightarrow Ce_2O_3 + CO$$

$$\text{“C”} + NO_2 \rightarrow CO + NO$$

$$Ce_2O_3 + NO_2 \rightarrow 2CeO_2 + NO$$

As seen from the data obtained (Table 3), thermal treatment of the catalyst CeO_2/θ-Al_2O_3 upon mixing with model soot (20% soot–80% CeO_2/θ-Al_2O_3) is accompanied by the ignition oxidation of soot at 360 °C and the exoeffect temperature is 415/625 °C. Deposition of Pt on CeO_2/θ-Al_2O_3 and following mixing this composition with soot (20% soot–80% Pt/CeO_2/θ-Al_2O_3) does not allow one to raise efficiency of the combustion of soot: the ignition temperature is 395 °C and the exoeffect temperature is 585/610 °C. This temperature is somewhat above than those in the presence of CeO_2/θ-Al_2O_3 (Table 3). Hence, it is reasonable to suppose that the catalyst efficiency to the soot oxidation is not improved in the presence of platinum. However study of the nature of the soot oxidation was organized for reception of the unambiguous answer depending on composition gas mixture in the presence of three catalysts: CeO_2/θ-Al_2O_3; Pt/CeO_2/θ-Al_2O_3 and Fe–Mn–K–O/γ-Al_2O_3.

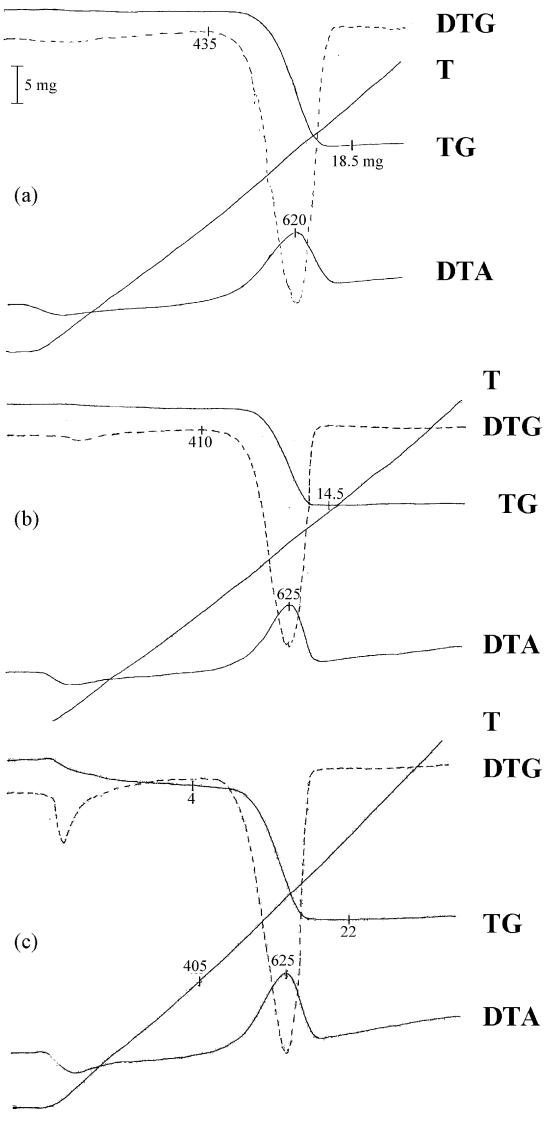

Fig. 5. The influence of support nature on the thermal behavior of the soot without (a) and in the presence of support: (b) soot–α-Al_2O_3; (c) soot-γ-Al_2O_3 compositions.

3.2. *The influence of the gas mixture composition on the oxidation of soot in the presence of catalysts*

Thermal behavior of the individual soot and the soot in the presence of catalysts is studied at different oxygen concentrations in the reaction mixture: 5% O_2/N_2, 10% O_2/N_2, 15% O_2/N_2 fed at 5 L air/h.

Table 4 shows that the soot oxidation in the mixture containing 5% O_2/N_2 is determined by the nature of the catalyst. The soot oxidation is observed at a higher temperature in the mixture than that in flowing air (Table 4), the oxidation efficiency being enhanced in the presence of the catalyst. A specific feature of all these thermal experiments is that the soot is not removed completely even at the temperature as high as 1000 °C. However, the proportion of removed soot increases in the presence of the catalyst.

An increase in the oxygen concentration has been expected to be accompanied by reduction of the ignition temperature and the exoeffect temperature for the soot and soot–catalyst compositions (Table 4). Depending on the catalyst nature, the soot ignition temperature decreases in the series:

Sample	$T_{ign.}$ (°C) in the gas mixtures			
	5% O_2/N_2	10% O_2/N_2	15% O_2/N_2	5 L air/h
Soot	570	510	465	435
Soot + CeO_2/θ-Al_2O_3	535	550	–	360
Soot + Pt–CeO_2/θ-Al_2O_3	540	530	465	395
Soot + Fe–Mn–K–O/γ-Al_2O_3	295; 610	305; 605	300	190; 340

Hence, the soot oxidation is more efficient at a higher oxygen concentration in the reaction mixture.

The influence of oxygen concentration in gas mixture on nature of the oxidation of soot is confirmed by kinetic method. The kinetics of the soot oxidation was studied in the presence of either α-Al_2O_3 or catalyst in the mixtures with different concentrations of oxygen, nitrogen and sulfur oxides. The main product of the soot oxidation is CO_2. The amount of CO does not exceed 0.5%, and CO is not observed at the presence of NO in the gas mixture.

Table 4
Thermal parameters of burning of the soot at various oxygen concentrations in the gas phase (soot weighed 20 mg, catalyst weight was 80 mg).

Catalyst	T_{endo} (°C)	Temp. of ignition, T_{DTG} (°C)	Temp. of exoeffect, T_{DTA} (°C)	Weight losses, TG	
				mg	%
Reaction mixture: 5%O_2/N_2					
Soot	–	570	–	11.0	55.0
20% Soot + 80% CeO_2/θ-Al_2O_3	120	535	880*	13.3	66.5
20% Soot + 80% Pt-CeO_2/θ-Al_2O_3	80*/235*	540	690*/865*	14.7	73.5
20% Soot + 80% Fe-Mn-K-O/γ-Al_2O_3	120	295, 610	440*; 835*	22.0	110
Reaction mixture: 10%O_2/N_2					
Soot	–	510	–	12.0	60.0
20% Soot + 80% CeO_2/θ-Al_2O_3	75*	550	745/920	12.2	61.0
20% Soot + 80% Pt-CeO_2/θ-Al_2O_3	85*/230*	530	665*/925*	15.4	77.0
20% Soot + 80% Fe-Mn-K-O/γ-Al_2O_3	70*	305, 605	440*; 700*/930*	19.2	96.0
Reaction mixture: 15%O_2/N_2					
Soot	–	465	665	18.0	90.0
20% Soot + 80% Pt-CeO_2/θ-Al_2O_3	90*	465	620	19.0	95.0
20% Soot + 80% Fe-Mn-K-O/γ-Al_2O_3	80*	300	445/600/630	22.5	112.5
5 L air/h					
Soot	–	435	620	18.5	92.5
20% Soot + 80% CeO_2/θ-Al_2O_3	75	360	415/625	16.5	82.3
20% Soot + 80% Pt-CeO_2/θ-Al_2O_3	75	395	585/610	19.2	96.0
20% Soot + 80% Fe-Mn-K-O/γ-Al_2O_3	–	190, 340	410, 540, 630	20.0	100

3.2.1. The influence of concentrations of oxygen and water vapor on the soot oxidation

Kinetic curves goes almost identical for the soot oxidation over three catalysts: CeO_2/θ-Al_2O_3, Pt-CeO_2/θ-Al_2O_3 and Fe–Mn–K–O/γ-Al_2O_3 (Fig. 6). However, the different behavior of the curves is observed for the process over Pt–CeO_2/θ-Al_2O_3, when a maximum at 200–220 °C is in the curve along with the main maximum. The presence of the additional maximum may be caused by elimination of the platinum oxide film in the presence of carbon. Treatment of kinetic curves for oxidation of the soot in the 'dry' and 'wet' mixtures over these catalysts reveals that the soot is oxidized at lower temperatures when the amount of water vapor is 10 vol.% in the gas mixture. Therefore, the presence of water vapor in the reaction mixture makes the process of the soot oxidation easier. The efficiency of the soot oxidation in the 'wet' mixture depending on the catalyst nature varies as follows:

$$\text{Fe–Mn–K–O/}\gamma\text{-Al}_2\text{O}_3 > \text{CeO}_2/\theta\text{-Al}_2\text{O}_3 \approx \text{Pt–CeO}_2/\theta\text{-Al}_2\text{O}_3 > \alpha\text{-Al}_2\text{O}_3$$

From the kinetic data (Fig. 6), the soot oxidation is completed at ca. 600–700 °C, while thermal studies demonstrate that only minor amount of the soot is removed at these temperatures in the oxygen–lean gas mixtures. The observed discrepancy may be caused by different rates of temperature elevation during thermal and kinetic experiments. This assumption may underlie the data on thermal analysis showing that an increase in the temperature elevation rate from 5 to 10 °C/min at otherwise identical conditions results in a rise of the soot ignition temperature from 400 to 435 °C.

Comparison of kinetic curves for the soot oxidation over three catalysts (Fig. 7) in the mixtures 5% O_2–10% H_2O–He (balance) and 10% O_2–10% H_2O–He (balance) reveals that the soot oxidation is more effective in the gas mixture containing 10% of O_2. Notice that under chosen experimental conditions (Fig. 7) the temperature to achieve the maximal soot oxidation rises depending on the catalyst nature, *viz.* Fe–Mn–K–O/γ-Al_2O_3 < CeO_2/θ-Al_2O_3 ≈ Pt–CeO_2/θ-Al_2O_3 < Al_2O_3. Thus, the kinetic studies with gas mixtures containing oxygen in different concentrations and 10% H_2O demonstrate that, first, the influence of the oxygen concentration on the process of soot oxidation weakens in the presence of water vapor and, second, Fe–Mn–K–O/γ-Al_2O_3 is the most effective among the catalysts under study for the soot oxidation at otherwise identical conditions.

3.2.2. The influence of nitrogen oxide concentration available in the oxygen-containing gas mixtures

The mixtures used for experimental studies of the influence of nitrogen oxide concentration on the oxidation of carbon-containing components in the presence of catalysts were the following: 10% O_2–*X* ppm NO–He (balance) (*X* = 250, 500, 750 ppm). The data obtained demonstrate that behavior of the kinetic curves for the soot oxidation over three catalysts in the mixture of 10% O_2–250 ppm NO–He (balance) (Fig. 8a) is practically identical. However, the different behavior is observed for Pt–CeO_2/θ-Al_2O_3. As mentioned above, that may happen due to removal of the platinum oxide film in the presence of carbon. An increase in the nitrogen oxide concentration leads to the further reduction of the temperature to achieve oxidation of the maximal amount of the soot (Fig. 8b and c). It is known that oxides of nitrogen (NO_2) is to be a more powerful oxidant than oxygen; therefore, it can oxidize the soot to CO and CO_2 at temperatures as low as 275–300 °C [28–32]. Emphasizing that an increase in the nitrogen oxide concentration contributes more to activation of the Pt-containing catalyst to improve its efficiency (Fig. 8). At the same time, comparative inspection of Fig. 8 reveals that the soot is oxidized at lower temperature over Fe–Mn–K–O/γ-Al_2O_3 than over Pt–CeO_2/θ-Al_2O_3.

Comparison of the oxidation temperatures of the identical soot in the mixtures 10% O_2–He (balance) and 10% O_2–250 ppm NO–He (balance) reveals that the presence of NO in amount of 250 ppm in the gas mixture favors a decrease in the oxidation temperature of the soot as follows:

The gas mixtures	The values of T_{max} for soot oxidation (°C)		
	CeO_2/θ-Al_2O_3	Pt–CeO_2/θ-Al_2O_3	Fe–Mn–K–O/γ-Al_2O_3
10% O_2–He (bal.)	596	225, 580	535
10% O_2–250 ppm NO–He (bal.)	550	225, 550	475/535

3.2.3. The influence of water concentration in the gas mixtures containing oxygen and nitrogen oxide

Kinetic studies on the influence of water that is contained along with oxygen and nitrogen oxide in the gas mixture on the process of catalytic oxidation of the soot showed (Fig. 9) that the basic oxidation parameters are not deteriorated. However, these parameters improved in the presence of water vapor in some cases.

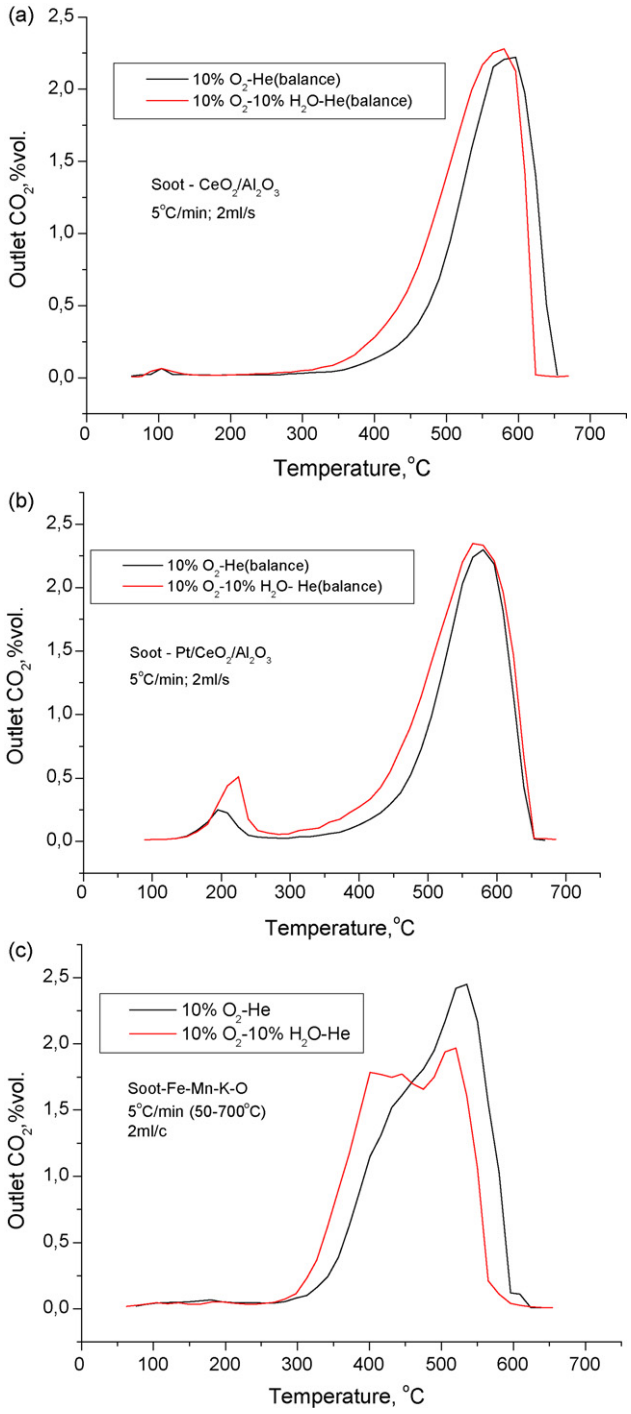

Fig. 6. The kinetic curves of the soot burning for different catalysts: (a) CeO_2/θ-Al_2O_3; (b) $Pt/CeO_2/\theta$-Al_2O_3; (c) Fe–Mn–K–O/γ-Al_2O_3 in the gas mixture containing: 10% O_2–He (balance) and 10% O_2–10% H_2O–He (balance).

3.2.4. *The influence of sulfur dioxide in the gas mixture containing oxygen, nitrogen oxide and water vapor*

The oxidation of soot does not considerably alter upon introduction of SO_2 in amount of 50 ppm into the gas mixture containing oxygen, nitrogen oxide and water (Fig. 10). The soot oxidation in the SO_2-containing gas mixture depends on the catalyst nature. T_{max} increases by 80 and 6 °C over CeO_2/θ-Al_2O_3 and Fe–Mn–K–O/γ-Al_2O_3 catalysts, respectively. T_{max} decreases by 10 °C over Pt–CeO_2/θ-Al_2O_3 catalyst. Probably, oxidation reaction of sulfur dioxide occurs in the presence of Pt ($SO_2 + (1/2)O_2 \xrightarrow{Pt} SO_3$).

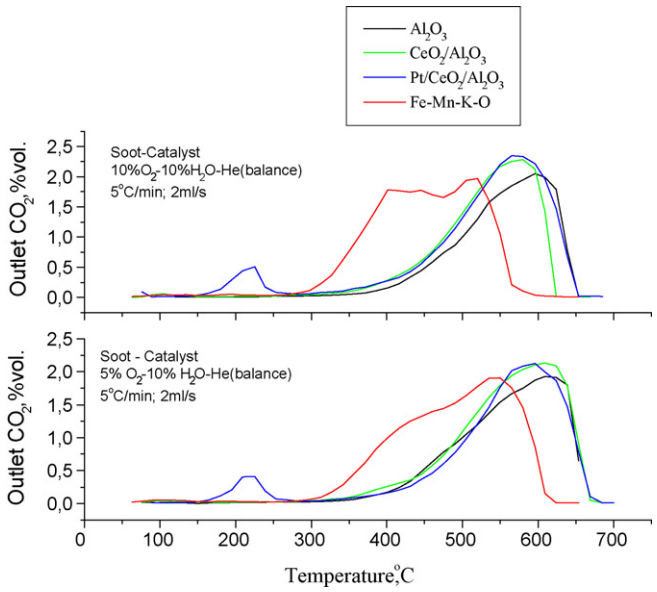

Fig. 7. The kinetic curves of the soot burning for different catalysts in the gas mixture containing 5% O_2–10% H_2O and 10% O_2–10% H_2O–He (balance).

At the same time, heat is evolved in this process and it provides slight decrease in T_{max}:

The gas mixtures	The values of T_{max} for soot oxidation (°C).		
	CeO_2/θ-Al_2O_3	Pt–CeO_2/θ-Al_2O_3	Fe–Mn–K–O/γ-Al_2O_3
10% O_2–500 ppm NO–He (bal.)	505	225, 535	445
10% O_2–500 ppm NO–10% H_2O–He (bal.)	505	225, 535	416
10% O_2–500 ppm NO–10% H_2O–50 ppm SO_2–He (bal.)	585	225; 525	420

Thus, the results obtained by kinetic studies of the soot oxidation in different gas mixtures, containing oxygen, nitrogen oxide, water vapor and sulfur dioxide in different concentrations lead us to conclude that, first, the influence of the oxygen concentration on the process of the soot oxidation is weakened in the presence of water vapor; second, the presence of NO in the gas mixture favors reduction of the temperature of the soot oxidation, the higher being nitrogen oxide concentration, the more pronounced the effect; third, the presence of sulfur dioxide has practically no impact on the process of the soot oxidation; fourth, Fe–Mn–K–O/γ-Al_2O_3 is the most effective among the catalysts under study for the oxidation of carbon-containing components at otherwise identical conditions.

The efficiency of Fe–Mn–K–O/γ-Al_2O_3 catalyst was confirmed for the soot oxidation (SDPF) obtained by washing away from a fragment of the filter using acetone that was subsequently to be then evaporated.

Non-isothermal treatment of SDPF (Fig. 11a) is accompanied by monotonous decreases of mass at temperatures above 125 °C. Its exoeffects are present on the DTA curve at 210 and 350 °C and the main exothermal effect is observed at 470/610 °C. Notice that a total weight loss in this soot sample weighing 20 mg is 87.5%, i.e. this value is less than the burnt amount of soot (92.5%) (Table 4). Hence, SDPF may comprise several carbon-containing fractions, although the data on weight losses at the related exoeffects (Table 5) indicate that the main fraction is graphite-like soot similar to the soot sample. A SDPF sample consists of globular particles of 20–50 nm in size (Fig. 11b); the particles are linked to one another to form extended chains and aggregates.

CeO_2/θ-Al_2O_3 is seen (Table 5) to have a minor effect on oxidation of SDPF: the ignition temperatures are 120 and 200 °C and

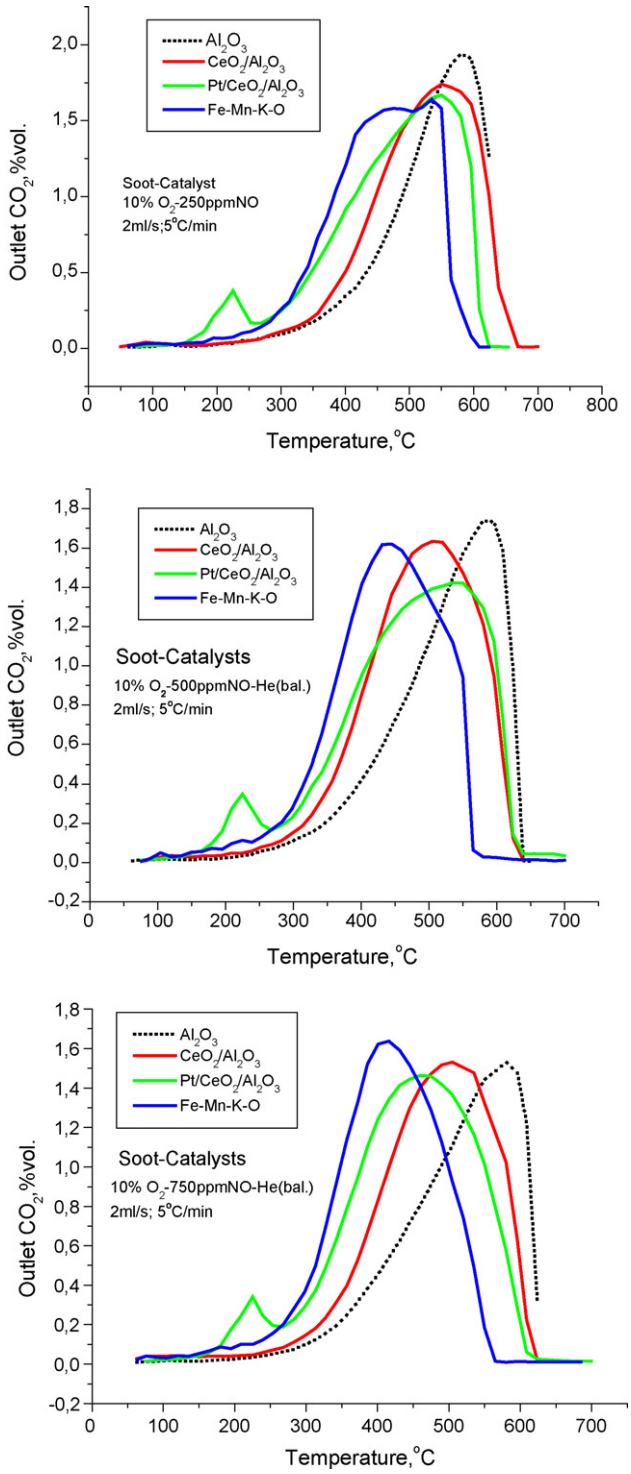

Fig. 8. The kinetic curves of the soot burning for different catalysts in the gas mixture containing 10% O_2–*X* ppm NO–He (bal.) (*X* = 250, 500, 750).

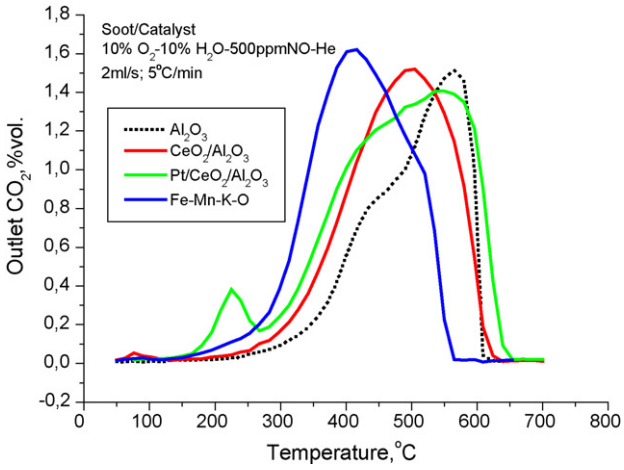

Fig. 9. The kinetic curves of the soot burning for different catalysts in the gas mixture containing 10% O_2–10% H_2O–500 ppm NO–He (bal.).

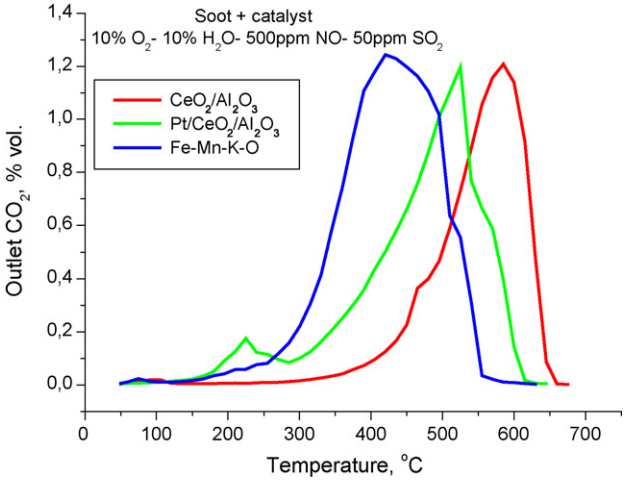

Fig. 10. The kinetic curves of the soot burning for different catalysts in the gas mixture containing 10% O_2–10% H_2O–500 ppm NO–50 ppm SO_2–He (bal.).

exoeffects are observed at 280/330 and 595 °C for the mixture of 20% SDPF–80% CeO_2/θ-Al_2O_3, while they are 125, 210, 350 and 470/610 for individual SDPF (Table 5). The process is more effective in the presence of Fe–Mn–K–O/γ-Al_2O_3; the exoeffect temperature decreases to 470 °C.

The data obtained by studying thermal behavior of the individual soot and the ones mixed with catalysts of various natures revealed that the oxidation is more effective in the presence of catalysts. For non-isothermal evolution of soot: $T_{ign.}$ = 435 °C; T_{exo} = 620 °C. These parameters alter in the presence of a catalyst. These values are changed in the presence of Fe–Mn–K–O/γ-Al_2O_3, and $T_{ign.}$ = 350 °C; T_{exo} = 420/540 °C. The soot picked up from a filter and referred to as SDPF is oxidized in the presence of Fe–Mn–K–O/γ-Al_2O_3 at temperatures: $T_{ign.}$ = 220 °C; T_{exo} = 330/400/470 °C.

Table 5
The influence of the nature catalyst on the character of SDPF oxidation.

Catalyst	T_{ads} (°C)/TG (%)	Temp. of ignition, T_{DTG} (°C)	Temp. of exoeffect, T_{DTG} (°C)	Weight losses "C", TG	
				mg	%
SDPF		**125, 210, 350**	**470/610**	**0.5, 2.0, 3.0, 12**	**87.5**
20% SDPF + 80% CeO_2/θ-Al_2O_3	130/3.0	200, 280/330	595	4.0, 14.0	90.0
20% SDPF + 80% Fe-Mn-K-O/γ-Al_2O_3	80/7.5	220	330/400/470	18.0	90.0

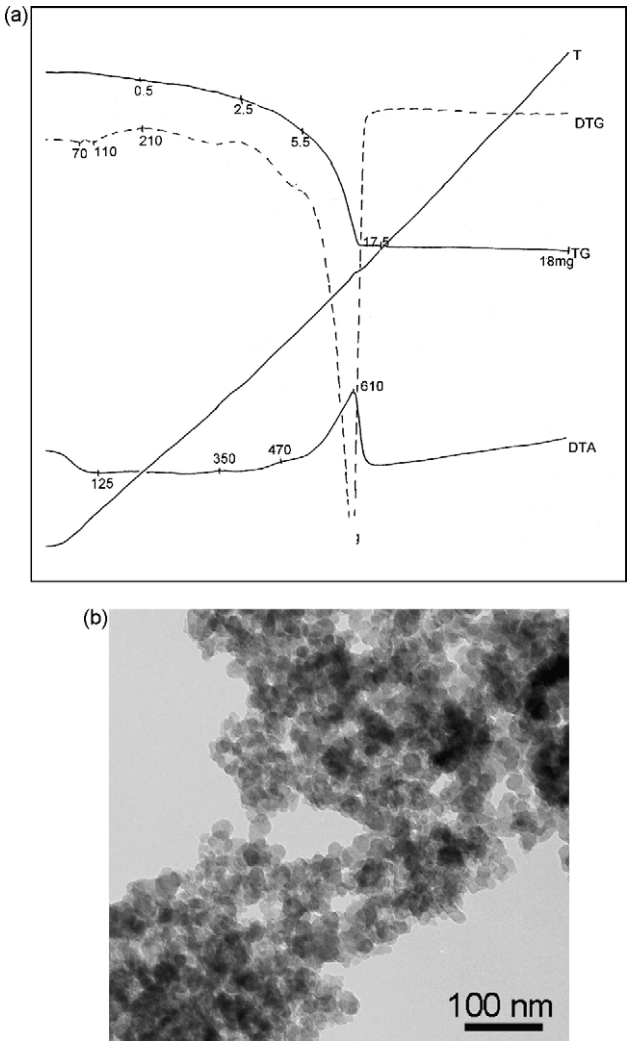

Fig. 11. Thermal parameters of burning of SDPF (a) and TEM image of SDPF (b).

The observed differences in their behavior during thermal treatment of the soot–catalyst compositions may be caused, first, by different states of active components in the catalyst surface second, by different phase compositions.

3.3. Surface concentration and chemical state of components in the Fe–Mn–K–O/SiO_2 catalyst

XPS spectra of Fe–Mn–K–O/SiO_2 catalysts containing 10 and 20 wt% of the active component were obtained in order to identify the surface concentration and chemical state of iron, manganese and potassium cations. The surface composition of the samples based on XPS measurements is summarized in Table 6. One can see that along with Fe, Mn, K and Si the surface layer of catalysts contains fair quantity of nitrogen. Nitrogen is a constituent of nitrate groups as indicated by the N1s binding energy equal to 407 eV. It is very important that the relative concentrations of iron and manganese on the surface are identical and independent of the supported component loading. At the same time, the relative concentrations of potassium and nitrogen are 1.5 and 2 times different, respectively. The surface Fe/Mn atomic ratio (of about 0.65) differs negligibly in the samples, however, it is much lower than their bulk ratio (of about 1.2).

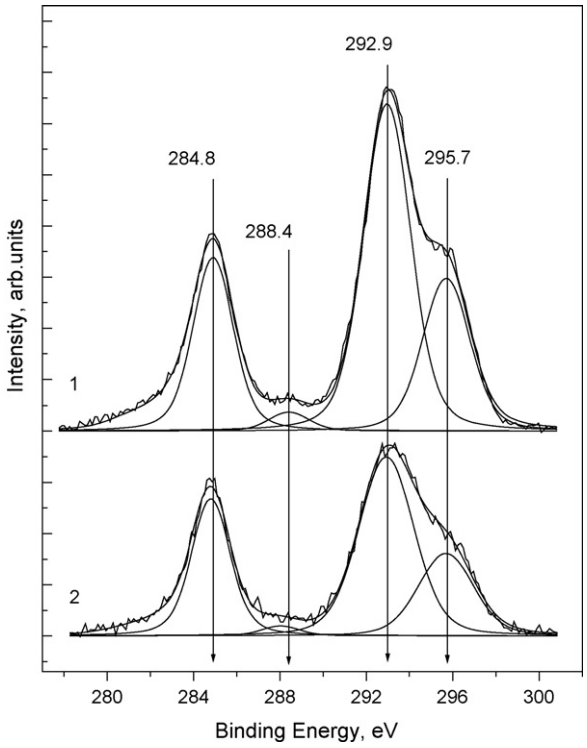

Fig. 12. C1s and K2p XPS spectra of Fe–Mn–K–O/SiO_2 catalysts containing 10.8 wt% (1) and 19.9 wt% (2) of the supported component.

Fig. 12 shows the C1s and K2p core-level spectra of the samples. An intense C1s peak at 284.8 eV is assigned to carbon of hydrocarbon compounds (C–C and C–H bonds) adsorbed on the surface after contacting with air. It is not excluded that hydrocarbon impurities are incorporated at the stage of sample synthesis from the reagents. A weak C1s peak at 288.4 eV relates to carbon of carbonate groups. A doublet at 292.9/295.7 eV relates to photoemission from $K2p_{3/2}$ and $K2p_{1/2}$ levels. The atomic ratio for carbon in CO_3 groups to potassium is 7.4 and 9.5 in the samples containing 10 and 20 wt% of the active component, respectively. Unfortunately, it is impossible to determine unambiguously the type of potassium compound because the $K2p_{3/2}$ binding energy has very low sensitivity to the nature of local chemical environment [33]. Nevertheless taking into account a low concentration of the carbonate groups we can speculate that potassium mainly belong to oxides like K_4MnO_4 and $KFeO_2$.

Fe2p and Mn2p core-level spectra of the samples under study are shown in Fig. 13. The Fe2p spectra show a complex structure consist of at least four peaks that is typical for Fe^{3+} compounds (Fig. 13a). According to literature data, two intensive peaks at 710.2 and 723.6 eV correspond to the $Fe2p_{3/2}$ and $Fe2p_{1/2}$ spin-orbit components, while two small extra-peaks at 718 and 732 eV are due to charge transfer multielectron transitions. It should be stressed that such satellites ca. 8 eV above the main lines are usually observed in the Fe2p spectra of Fe^{3+} compounds like [34–36]. In the spec-

Table 6
Chemical composition of surface layer of Fe–Mn–K–O/SiO_2 catalysts calcined at 400 °C based on XPS data.

Composition (mol.%)	[Fe]/[Si]	[Mn]/[Si]	[K]/[Si]	[N]/[Si]	[Fe]/[Mn]
2.45Fe_2O_3–2Mn_2O_3–1.65K_2O–93.9SiO_2 (Fe/Mn = 1.22)	0.11	0.16	0.42	0.10	0.68
4.8 Fe_2O_3–3.9Mn_2O_3–2.1 K_2O–89.2SiO_2 (Fe/Mn = 1.23)	0.10	0.16	0.27	0.05	0.63

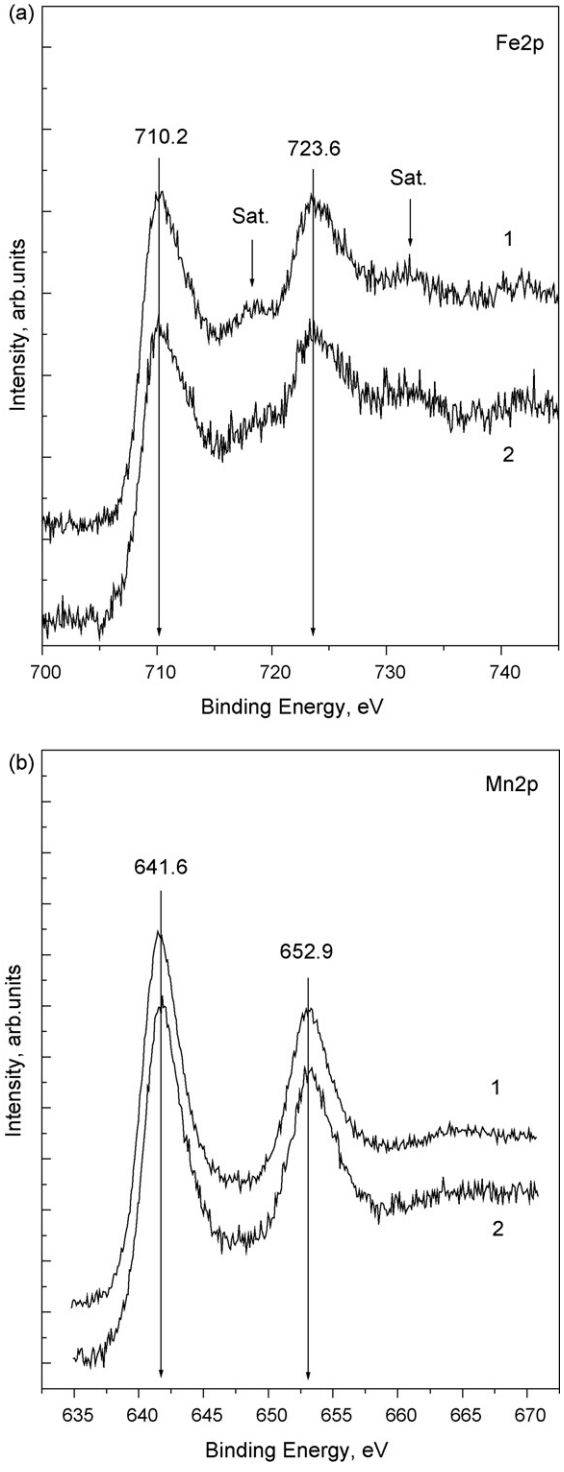

Fig. 13. Fe2p (a) and Mn2p (b) XPS spectra of Fe–Mn–K–O/SiO_2 catalysts containing 10.8 wt% (1) and 19.9 wt% (2) of the supported component.

tra of FeO the satellites locate ca. 6 eV above the main lines, and no satellites are observed in the spectra of Fe_3O_4 and metallic iron. The values of the $Fe2p_{3/2}$ binding energies for FeO, Fe_3O_4, Fe_2O_3 and FeOOH are in the ranges 709.1–710.65, 707.9–710.7, 710.6–711.5 and 710.2–711.05 eV, respectively [34–36]. Therefore, taking into account the satellite structure in the Fe2p spectra we suppose that the predominant oxidation state of iron on the catalysts surface is Fe^{3+}. The understated value of the $Fe2p_{3/2}$ binding energy for the catalysts under study is due to interaction iron cations with

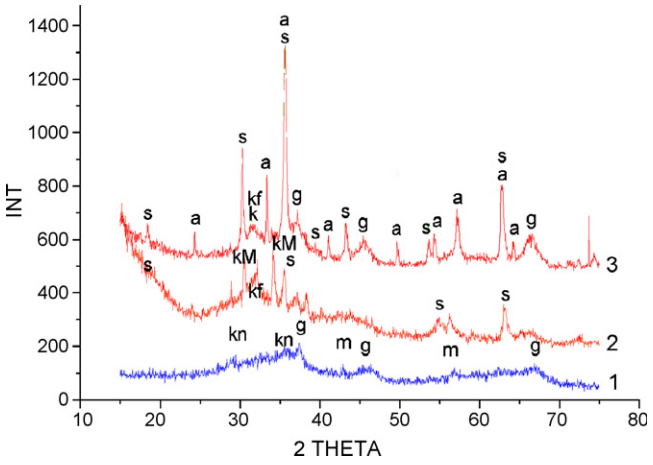

Fig. 14. XRD pattern of samples: (1) Fe–Mn–K–O/γ-Al_2O_3—starting, 1000 °C, air; (2) Fe–Mn–K–O/γ-Al_2O_3 + soot, 1000 °C, air; (3) Fe–Mn–K–O/γ-Al_2O_3 + soot, 1000 °C, 5% O_2. The following designations are used: g, γ-Al_2O_3; a, α-Fe_2O_3; s, spinel based on Fe_3O_4; Kf, $KFeO_2$; K, carbonate potassium; Kn, nitrate potassium; kM, K_4MnO_4; m, MnO_2.

potassium or manganese cations in a double oxides structure. For example, the $Fe2p_{3/2}$ binding energy for $NiFe_2O_4$ and $CoFe_2O_4$ is lower on 0.4 eV then for Fe_2O_3 [34].

The Mn2p core-level spectra of the samples are practically identical (Fig. 13b). Spectra due to spin-orbital splitting consist of two wide peaks which correspond to $Mn2p_{3/2}$ and $Mn2p_{1/2}$ components. The $Mn2p_{3/2}$ binding energy is about 641.6 eV. This value is in the range of that reported for Mn_2O_3 (641.0–641.8 eV) and MnO_2 (641.7–642.6 eV) [37–39]. It points out that manganese on the catalysts surface is in both Mn^{3+} and Mn^{4+} oxidation states.

The results of XPS study have revealed that (1) the surface concentrations of iron and manganese are independent of the active component loading in the catalyst and (2) both iron and manganese are in their maximal oxidation states on the surface that, seemingly, affects the activity of these catalysts in the soot oxidation.

3.4. Phase composition of supports and catalysts before and after soot burning

Phase composition of the catalysts was studied before and after soot burning. Three sample series were characterized before and after burning of the soot in the gas mixture (5% O_2/N_2) fed at 5 L air/h (Table 7). It follows from comparison of the results obtained for Fe–Mn–K(Cs)–O/γ-Al_2O_3 and Fe–Mn–K(Cs)–O/SiO_2 catalysts that the support nature and preparation procedure (deposition or impregnation) do not affect considerably the phase composition of the initial catalysts. All the initial samples are poorly crystalline. These samples consist of several phases (Table 7). Diffuse lines are seen in the diffraction pattern (Fig. 14, curve 1) against the background form of the support (γ-Al_2O_3, JCPDS, 10-0425). The lines are around the position of the most intense lines of undecomposed potassium nitrate, dispersed spinel like γ-Fe_2O_3 (JCPDS, 24-0081) and dispersed low-temperature phase γ-MnO_2 (JCPDS, 04-0779). For K- and Cs-containing catalysts, the diffraction lines are assigned to potassium and cesium nitrates, respectively. No formation of potassium or cesium ferrite phases is detected in some cases of K- and Cs-containing catalysts, respectively. It is known that potassium ferrite is formed at $T \sim 600$–620 °C, however, it is decomposed into iron and potassium oxides on cooling. Potassium oxide is rapidly transformed into potassium carbonate (or hydroxycarbonate) in air. Probably, potassium ferrite, manganese oxide and iron oxide are not yet crystallized at the temperature below 600 °C. The related diffraction pattern indicates the X-ray amorphous structure.

Table 7
Phase composition of the catalysts before and after burning of the soot.

Catalyst	Initial sample	After treatment of the soot by flowing 5% O_2/N_2 at 1000 °C	After treatment of the soot by air fed at 5 L/h at 1000 °C
Fe–Mn–O/γ-Al_2O_3	Poorly crystalline products of nitrates decomposition; γ-Al_2O_3	–	Mn_2O_3 (probably, promoted by Fe^{3+}); Fe_2O_3; $MnFe_2O_4$
Fe–Mn–K-O/γ–Al_2O_3		Trace of $KFeO_2$ or its decomposition products; γ-Al_2O_3; $(Fe_xMn_{1-x})_3O_4$; α-Fe_2O_3	$KFeO_2$ or its decomposition products, K_4MnO_4, γ-$(FeMnAl)_2O_3$
Fe–Mn–Cs-O/γ-Al_2O_3		–	Mn_2O_3 (probably, promoted by Fe^{3+}); Fe_2O_3;
Fe–Mn–K–O/SiO_2		–	Mn_2O_3 (probably, promoted by Fe^{3+}); α-Fe_2O_3; $MnFe_2O_4$; $Mn_2O_3 \gg (\alpha\text{-}Fe_2O_3 + MnFe_2O_4)$; beginning of quartz crystallization
CeO_2/θ-Al_2O_3	CeO_2: $a = 0.541 \pm 0.002$ nm; $D = 9.5$ nm; Al_2O_3	CeO_2: $a = 0.541 \pm 0.002$ nm; $D = 22$ nm; Al_2O_3	–
Pt–CeO_2/θ-Al_2O_3	CeO_2: $a = 0.541 \pm 0.002$ nm; $D = 9.5$ nm; Al_2O_3	CeO_2: $a = 0.541 \pm 0.002$ nm; $D = 22$ nm; Al_2O_3; Pt: $D = 8$ nm	–

After burning of the soot at 1000 °C, the phase composition depends on the oxygen concentration in the gas phase (Fig. 14, curves 2 and 3). When the soot is burnt on heating in air, the diffraction pattern (Fig. 14, curve 2) features lines of dispersed spinel γ-$(FeMnAl)_2O_3$, which are shifted with respect to the ones of pure γ-Al_2O_3. The lines of a well crystalline phase which may be assigned to K_4MnO_4 (JCPDS, 31-1051) and the lines which may be assigned to $KFeO_2$ (JCPDS, 39-0891) or its decomposition products such as $K_2CO_3 \cdot nH_2O$ (JCPDS 11-0665) or K_2CO_3 (JCPDS, 27-1348) are observed. The phase composition is different when the soot is oxidized in the gas mixture containing 5% O_2/N_2. The lines of K_4MnO_4 disappear in the diffraction pattern (Fig. 14, curves 3), however, the lines which are related to well crystalline phases such as hematite α-Fe_2O_3 (JCPDS, 33-0664) and spinel $(Fe_xMn_{1-x})_3O_{4+\gamma}$ based on the magnetite Fe_3O_4 structure (JCPDS, 19-0629) appear. Again, similar to the patterns of samples calcined in air, there are lines of the dispersed support phase γ-Al_2O_3 and $KFeO_2$ or its decomposition products such as $K_2CO_3 \cdot nH_2O$ and K_2CO_3. The samples of Fe–Mn–K–O/γ-Al_2O_3 + soot are different in the ratio of phases α-Fe_2O_3 and $(Fe_xMn_{1-x})_3O_{4+\gamma}$: the phase of $(Fe_xMn_{1-x})_3O_{4+\gamma}$ predominates after the soot burning in the gas mixture containing 5% O_2/N_2 (Fig. 14, curve 3). The reason may be a considerable influence of the gas phase on the valent state of manganese ions in the spinel phase.

Two phases, CeO_2 and Al_2O_3, are observed in the initial CeO_2/θ-Al_2O_3 sample (Table 7). The strong dissipative effect of cerium atoms makes the diffraction lines of the CeO_2 phase (cell constant close to the reference data, $a = 0.541 \pm 0.002$ nm, JCPDS, 43-1002) predominant in the diffraction pattern. The particles are 9.5 nm in average size. For alumina, only line is practically observed at $d = 0.1388 \pm 0.0003$ nm; it is hardly possible to use this line for identification of the alumina phase since it is characteristic of all the alumina modifications. When the soot has been oxidized at 1000 °C, the samples are practically identical in the composition and almost not differ from the initial sample (Table 7). The intense lines of the CeO_2 phase with cell constant $a = 0.541$ nm and a line at $d = 0.1388$ nm related to alumina are observed in the diffraction pattern, the line of alumina being more pronounced (at the same position though), however, the lines of CeO_2 considerably narrower that indicates an increase of the crystallites to 22 nm in size independently of the burnt component.

Phases of CeO_2 and Al_2O_3 are also identified in the initial Pt–CeO_2/θ-Al_2O_3 (Table 7), however, the alumina phase is some more evident than that in CeO_2/θ-Al_2O_3. The CeO_2 particles are also 9.5 nm in average size. The samples are practically identical after the soot have burnt at 1000 °C, they comprise phases of CeO_2 ($a = 0.541$ nm, average CSR is 17.5 nm), alumina and platinum ($a = 0.3923 \pm 0.0002$ nm, average CSR is 8 nm) (Table 7).

The results demonstrate that the phase composition of catalysts under study is determined by following factors: the nature of the active component, preparation procedure and treatment temperature and to a lesser degree the presence of the soot. Comparison of the related TA and XRD data shows that the most active systems to the soot oxidation are catalytic systems containing either poorly crystallized phases, or spinel structures $[(Fe_xMn_{1-x})_3O_{4+\gamma}]$, or alkali metal ferrites or manganates. Supposedly, these compounds provide a higher mobility of surface oxygen due to the presence of weakly bound or overstoichiometric oxygen.

4. Conclusions

Thermal behavior of the soot is studied in the absence and in the presence of catalysts in an atmosphere of air fed at the rate of 5 L/h. The soot consists of globular particles of 20–50 nm in size. The soot particles are linked to one another to form extended chains and aggregates. For non-isothermal evolution of the soot: $T_{ign.} = 435$ °C and $T_{exo} = 620$ °C; the soot picked up from a filter and referred to as SDPF consists of several carbon fractions oxidized at 125, 210, 350 and 610 °C, the graphite-like soot being the main component. These parameters alter in the presence of a catalyst.

Physicochemical and catalytic properties of compositions Fe(Ce)–Mn–O/support (γ-,θ-, α-Al_2O_3, SiO_2 as the support) and Pt/CeO_2/θ-Al_2O_3 for the soot oxidation were investigated. The phase composition of the initial catalysts was shown to depend mainly on the nature of the active component, preparation conditions and treatment temperature. Non-isothermal treatment of a soot–catalyst mixture at the temperature up to 1000 °C resulted in a change in the phase composition which depends mainly on the final treatment temperature. The catalyst surface area was determined by the support nature. The process of the soot oxidation is thought to involve oxygen from the catalyst surface. The higher proportion of weakly bound surface oxygen, the higher was the catalytic activity.

The catalytic activity in the soot oxidation depends on the gas mixture composition. An increase in the oxygen concentration from 5% O_2/N_2 to 15% O_2/N_2 is shown to lead to a decrease of oxidation temperatures of the soot. The influence of the oxygen concentration on the process of oxidation of hydrocarbon components becomes weaker in the presence of water vapor. It is established that the presence of NO in the gas mixture favors a decrease in the oxidation temperature of the soot, the higher being the nitrogen oxide concentration, the more pronounced effect. Introduction of SO_2 in amount of 50 ppm in the gas mixture has no noticeable effect on the process of soot oxidation.

Among the catalysts under study, Fe–Mn–K(Cs)/γ-$Al_2O_3(SiO_2)$ is the most effective to oxidation of hydrocarbon-containing components at otherwise identical conditions. For non-isothermal evolution of soot–Fe–Mn–K–O/γ-Al_2O_3 and SDPF–Fe–Mn–K–O/γ-Al_2O_3 mixtures: $T_{ign.} = 350$ °C; $T_{exo} = \underline{420}/540$ °C for soot and $T_{ign.} = 220$ °C; $T_{exo} = 330/400/\underline{470}$ °C for SDPF.

References

[1] S. Kalvert, G.M. Inglund (Eds.), Atmospheric Protection form Industrial Contaminators Reference Book, Metallurgia, Moscow, 1988, pp. 636–666.
[2] D.W. McKee, C.L. Spiro, P.G. Kosky, E.J. Lamby, Fuel 64 (1985) 805–809.
[3] D.W. McKee, Fuel 62 (1983) 170–175.
[4] D.W. McKee, C.L. Spiro, P.G. Kosky, E.J. Lamby, in: P.J. Reucroft, P.C. Eklund, C.C. Banks (Eds.), Proceed. of the 17th Biennial Conference on Carbon, Kentucky, June 16–21, 1985, pp. 184–185.
[5] D.W. McKee, Carbon 25 (1987) 587–588.
[6] J.J. Sytse, Diesel Exhaust After treatment. Development of Catalytic Systems for Diesel Particulate Oxidation, Delft University of Technology, 1999, pp.148–164.
[7] B.A.A.L. Van Setten, C.G.M. Spitters, J. Bremmer, A.M.M. Mulders, M. Makkee, J.A. Moulign, Appl. Catal. B 42 (2002) 337–347.
[8] D. Courcot, E. Abi-Aad, S. Capelle, A. Aboukais, Stud. Surf. Sci. Catal. 116 (1998) 625–634.
[9] P. Ciambelli, P. Corbo, M. Gambino, V. Palma, S. Vaccaro, Catal. Today 27 (1996) 99–106.
[10] M. Ambrogio, G. Saracco, V. Specchia, Chem. Eng. Sci. 56 (2001) 1613–1621.
[11] S. Liu, A. Obuchi, J. Oi-Uchisawa, T. Nanba, S. Kushiyama, Appl. Catal. B 30 (2001) 259–265.
[12] J.H. Johnson, S.T. Bagley, L.D. Gratz, D.G. Leddy, SAE paper 940233 (1994).
[13] V.P. Zuev, V.V. Mikhailov, Production of Soot, Khimiya, Moscow, 1970, pp. 9–13.
[14] R.J. Locker, N. Gunasekaran, C. Sawyer, Soc. Automot. Eng. (2002) 1–12.
[15] A. Trovarelli, M. Boaro, E. Rocchini, C. de Leitenburg, G. Dolcetti, J. Alloys Compd. 323–324 (2001) 584–591.
[16] K. Tikhomirov, O. Krocher, M. Elsener, A. Wokaun, Appl. Catal. B 64 (2006) 72–78.
[17] W.J. Price, Analytical Atomic-Absorption Spectroscopy, 1976 (New York).
[18] JCPDS, PCPDF, Win. Ver 1. 30, JCPDS ICDD, Swarthmore, PA, USA, 1997.
[19] N.E. Buyanova, A.P. Karnaukhov, Yu.A. Alabuzhev, Determination of Specific Surface Area of Dispersed and Porous Materials, Institute of Catalysis, Novosibirsk, 1978.
[20] D.G. Klisurski, I.G. Mitov, T.T. Tomov, Proceedings of IN Int. Symp. on Heterogeneous Catalysis, Varna, 2–5 October, 1979, pp. 207–212.
[21] V.G. Milt, M.L. Pissarello, E.E. Miro, C.A. Quercini, Appl. Catal. B 41 (2003) 397–414.
[22] G. Neri, G. Rizzo, S. Galvagno, A. Donato, M.G. Musolino, R. Pietropaolo, Appl. Catal. B 42 (2003) 381–391.
[23] S. Kureti, W. Weisweiler, K. Hizbullah, Appl. Catal. B 43 (2003) 281–291.
[24] A. Bueno-Lopez, K. Krishna, M. Makkee, J.A. Moulijn, J. Catal. 230 (2005) 237–248.
[25] E. Aneggi, C. de Leitenburg, G. Dolcetti, A. Trovarelli, Catal. Today 114 (2006) 40–47.
[26] I. Atribak, A. Bueno-Lopez, A. Garcia-Garcia, Catal. Commun. 9 (2008) 250–255.
[27] S. Damyanova, J.M.C. Bueno, Appl. Catal. A: Gen. 253 (2003) 135–150.
[28] A. Setiabudi, B.A.A.L. van Setten, M. Makkee, J.A. Moulijn, Appl. Catal. B 35 (2002) 159–166.
[29] A. Setiabudi, J. Chen, G. Mul, M. Makkee, J.A. Moulijn, Appl. Catal. B 51 (2004) 9–19.
[30] Holleman, Text-Book of Inorganic Chemistry, John Wiley & Sons, 1903.
[31] B.J. Cooper, J.E. Thoss, SAE 890404, 1989 (Detroit).
[32] A. Setiabudi, M. Makkee, J.A. Moilijn, Appl. Catal. B 42 (2003) 35–45.
[33] W.E. Morgan, J.R. van Wazer, W.J. Stec, J. Am. Chem. Soc. 95 (1973) 751–755.
[34] N.C. McIntyre, D.G. Zetaruk, Anal. Chem. 49 (1977) 1521–1529.
[35] P.C.J. Graat, M.A.J. Somers, Appl. Surf. Sci. 100–101 (1996) 36–40.
[36] M. Descostes, F. Mercier, N. Thromat, C. Beaucaire, M. Gautier-Soyer, Appl. Surf. Sci. 165 (2000) 288–302.
[37] C. Colmenares, S. Deutsch, C. Evans, A.J. Nelson, L. Terminello, J. Reynolds, J.W. Roos, I.L. Smith, Appl. Surf. Sci. 151 (1999) 189–202.
[38] H.W. Nesbitt, D. Banerjee, Am. Miner. 83 (1998) 305–315.
[39] V. Di Castro, G. Polzonetti, J. Electron Spectrosc. Relat. Phenom. 48 (1989) 117–123.